Explicitly correlated three-dimensional potential-energy surface of the thiazyl-hydride–helium weakly bound system and implications for HSN detection

Y. Ajili
Laboratoire Modélisation et Simulation Multi Echelle, Université Paris-Est, MSME UMR 8208 CNRS, 5 Boulevard Descartes, 77454 Marne-La-Vallée, France

D. Ben Abdallah
Department of General Studies, Riyadh Corporation of Technology, Technical and Vocational Training Corporation, P.O. Box 42826, Riyadh 11551, Kingdom of Saudi Arabia

M. Mogren Al-Mogren
Chemistry Department, Faculty of Science, King Saud University, P.O. Box 2455, Riyadh 11451, Kingdom of Saudi Arabia

F. Lique
LOMC-UMR 6294, CNRS, Université du Havre, 25 Rue Philippe Lebon, Boîte Postale 540, 76058, Le Havre, France

J. S. Francisco
Department of Chemistry and Department of Earth and Atmospheric Science, Purdue University, West Lafayette, Indiana 49707, USA

M. Hochlaf*
Laboratoire Modélisation et Simulation Multi Echelle, Université Paris-Est, MSME UMR 8208 CNRS, 5 Bd Descartes, 77454 Marne-La-Vallée, France

(Received 9 June 2016; published 19 July 2016)

The intermonomer three-dimensional potential-energy surface (3D PES) of the thiazyl-hydride–helium (HSN-He) weakly bound molecular system is generated using the explicitly correlated coupled-cluster method with single, double, and perturbative triple excitations. The 3D PES is mapped in Jacobi coordinates. This potential-energy surface shows a unique potential well at planar configurations. The depth of this potential is 74.4 cm^{-1}. This 3D PES is incorporated into a close-coupling and coupled-states quantum dynamical treatment of nuclear motions to deduce the rotational (de-)excitation of HSN by He for energies up to 1400 cm^{-1}. After averaging over a Maxwell-Boltzmann distribution, the collisional rate coefficients are derived for temperatures ranging from 5 to 200 K. These data are essential for the identification of HSN molecules in astrophysical media. A comparison between thionitrosyl-hydride—He and HSN-He is performed.

DOI: 10.1103/PhysRevA.94.012512

I. INTRODUCTION

Only a few molecules containing both sulfur and nitrogen are detected in astrophysical media. To date, the list of detected molecules is restricted to the diatomic nitrogen sulfide (SN [1]) and the tetratomics isothiocyanic acid (HNCS) [2]) and thiocyanic acid (HSCN [3]). This list is relatively short when one considers the rich chemistry occurring in these media and where for instance the SN diatomic can be involved. Surprisingly, these observations do not include any triatomic SN-containing molecules, even the thiazyl hydride (HSN) or thionitrosyl hydride (sulfimide, HNS) species that may be formed after reactive collisions or radiative attachment reactions between SN and the H atom. Recent studies have shown that favorable reaction pathways for bimolecular collisions between SN and H exist and these can lead to the formation of HSN and HNS triatomics [4]. Bimolecular H-H^- + SN^--SN reactions followed by electron detachment have been suggested to form HSN or HNS [5]. Although the rates of such reactions are slow and/or the abundance of the SN^- anion for the latter process is low, both HNS and HSN molecular species are suspected to be present and hence detectable in astrophysical media at least where SN is definitely identified [1]. Detection of HNS and HSN, however, requires an accurate set of rotational and vibrational spectroscopic parameters, and information regarding their molecular stabilities, reaction probabilities, and radiative and collisional excitation rates with the most abundant interstellar species (i.e., H, He, H_2, and free electrons) under the physical conditions of the interstellar medium [6,7]. High-resolution telescopes are capable of detecting these molecules and of giving insights into their abundances after analysis of the corresponding spectral lines [8].

Without spectroscopic laboratory measurements of HNS and HSN, it is difficult to identify their molecular lines in astronomical spectral survey. In 2014, Ben Yaghlane *et al.* provided accurate geometric parameters and the rovibrational structure of both HNS and HNS molecular species using state-of-the art theoretical and computational approaches [9]. Ajili *et al.* [10] examined the rotational (de)excitations of thionitrosyl hydride, HNS, by He. In the present contribution, the three-dimensional

*Corresponding author: hochlaf@univ-mlv.fr

(3D) intermononomer interacting potential of the HSN-He complex is presented in Jacobi coordinates. The electronic computations are carried out using the explicitly correlated coupled-cluster approach with single, double, and perturbative treatment of triple excitations [CCSD(T)-F12] [11,12] in conjunction with the augmented correlation-consistent polarized valence triple-zeta (aug-cc-pVTZ) basis set [13,14].

Dynamical computations of the nuclear motions on this potential are studied, after which, the rotational (de)excitation collision rate coefficients of HSN by He are deduced. Note that the dominant collisional partner in the cold interstellar medium is para-H_2. For heavy molecules such as HSN, the use of He as a template for para-H_2 represents a reasonable approximation for the estimation of the collisional data. Such treatment is found to lead to limited uncertainties whereas the cost of the computation is strongly reduced [8]. This study focuses on rotational (de-)excitation at low-temperature collision rates, i.e., well below the threshold for the excitation of the vibrational modes of HSN ($\tilde{X}\,^1A$) ($\nu_1 = 2031$, $\nu_2 = 1005$, and $\nu_3 = 1162\,\mathrm{cm}^{-1}$) [9]. Hence, the HSN molecule is considered as a rigid rotor. In 2005, Faure *et al.* [15] showed that several choices for the geometry of the triatomic molecule are possible such as the r_e or r_0 structures, the latter being seemingly preferable. Since there appear to be no experimental structural data on HSN, the internal coordinates (r_{HS}, r_{SN}, α) of HSN are fixed at their equilibrium geometry as computed at the CCSD(T)-F12 level with the cc-pVQZ-F12 basis set [9]: $r_{\mathrm{HS}} = 2.657$ bohr, $r_{\mathrm{SN}} = 2.827$ bohr, and $\alpha = 109.9°$. Together with the spectroscopic parameters, the calculated collision rate coefficients should help in the identification of HNS in astrophysical media.

II. INTERMOLECULAR POTENTIAL-ENERGY SURFACE OF HSN-He COMPLEX

Electronic computations are performed using the MOLPRO package (version 2012) [16] in the C_1 point group symmetry. Preliminary CASSCF computations that were carried out showed that the weight of the dominant configuration for the ground state is around 0.93 for all investigated geometries of the HSN-He complex. This validates the use of monoconfigurational methods for the generation of the potential-energy surfaces for the HSN-He complex. Using the explicitly correlated coupled-cluster [CCSD(T)-F12] method, the aug-cc-pVTZ basis set was used for H, He, S, and N atoms. The MOLPRO default choices for the density fitting and resolution of identity basis sets were applied [17]. In a series of papers, this methodology has been shown to generation accurate multidimensional potential surfaces of weakly bound complexes [18–24]. Indeed, we established that the CCSD(T)-F12 with aug-cc-pVTZ potential-energy surfaces are close to those computed using the standard coupled-cluster approach and a complete-basis-set (CBS) extrapolation limit.

The ground state of the HSN-He complex is of singlet spin multiplicity. It correlates with the HSN ($\tilde{X}\,^1A$) + He asymptote at large intermonomer separation. The energy of this asymptote is taken as reference. For the calculations of the interaction potential between HSN and He, Jacobi coordinates R,θ,ϕ, as shown in Fig. 1, are used. They are defined with respect to the molecular fixed principal inertia axes (Gx, Gy, Gz) whose origin coincides with the center-of-mass of HSN, G. These axes are placed along the three principal directions of inertia of the HSN asymmetric-top molecule. R connects G and He; θ is the angle between R and the (Gz) axis, and ϕ is the angle between the molecular plane (Gxz plane) and the axis joining the center of mass of the molecule HSN to thate of the He atom. The (Gx), (Gy), and (Gz) axes are placed along the three principal directions of inertia of HSN molecule.

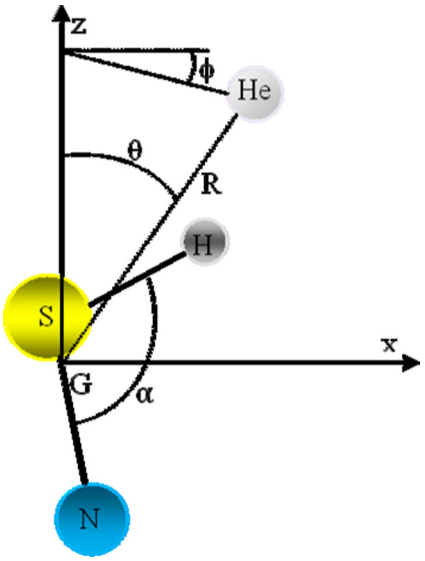

FIG. 1. Jacobi coordinates of HSN-He system with respect to the HSN center of mass G and principal axes (Gx, Gy, Gz). The planar configuration (Gxz plane) corresponds to $\phi = 0°$.

This 3D potential-energy surface (PES) is constructed with 9139 nonequivalent *ab initio* geometries where 37 values for the scattering coordinate R (from $4.25a_0$ to $100a_0$) are assigned, and 19 and 13 values are assigned (from 0° to 180°) for the angles θ and ϕ, respectively. The grids on θ and ϕ are uniform with steps of 10 and 15°, respectively. R is set to [4.25, 4.5, 4.75, 5, 5.25, 5.5, 5.75, 6, 6.25, 6.5, 6.75, 7, 7.25, 7.5, 7.75, 8, 8.25, 8.5, 8.75, 9, 9.25, 9.5, 9.75, 10, 10.5, 11, 12, 13, 14, 16, 18, 20, 25, 30, 40, 50, 100] (in units of a_0; $1\,a_0 = 1$ bohr $= 0.5292$ Å). For mapping the 3D PES, a relatively large grid of R coordinates is used for several angular orientations in order to account for possible anisotropy of this potential. For each nuclear configuration, the interaction potential $V(R,\theta,\phi)$, is corrected by the basis-set superposition error (BSSE) using the Boys and Bernardi [25] counterpoise formula:

$$V(R,\theta,\phi) = E_{\mathrm{HSN-He}}(R,\theta,\phi) - E_{\mathrm{HSN}}(R,\theta,\phi) - E_{\mathrm{He}}(R,\theta,\phi), \quad (1)$$

where $E_{\mathrm{HSN-He}}(R,\theta,\phi)$, $E_{\mathrm{HSN}}(R,\theta,\phi)$, and $E_{\mathrm{He}}(R,\theta,\phi)$ are the total electronic energies of the HSN-He cluster and the HNS and He subsystems, respectively, and where all energies are computed in the full basis set of HSN-He.

Because of the non-size-consistency of the CCSD(T)-F12 method [12], the generated potential is shifted up by $\sim 4.76\,\mathrm{cm}^{-1}$ (its absolute value for $R = 100\,a_0$). Then we deduced an analytic expansion of this 3D PES, where the

TABLE I. Equilibrium geometries (distances in units of a_0) and depth of the potential wells (V, cm^{-1}) of the minimal structures of the HSN-He 3D PES for $\phi = 0°$, $\phi = 90°$, and $\phi = 180°$.

$\phi = 0°$					
$\theta = 5°$		$\theta = 103°$		$\theta = 180°$	
R	V	R	V	R	V
7.15	−45.04	6.15	−74.39	8.35	−25.09
$\phi = \mathbf{90}°$					
$\theta = 0°$		$\theta = 121°$			
R	V	R	V		
7.15	−44.33	6.95	−32.36		
$\phi = \mathbf{180}°$					
$\theta = 0°$		$\theta = 75°$		$\theta = 180°$	
R	V	R	V	R	V
7.15	−44.33	6.55	−36.01	8.35	−25.08

ab initio energies were fitted to the following formula:

$$V(R,\theta,\phi) = \sum_{l=0}^{l_{\max}} \sum_{m=0}^{m_{\max}} v_{lm}(R) \frac{Y_{l,m}(\theta,\phi) + (-1)^m Y_{l,-m}(\theta,\phi)}{1+\delta_{m0}}, \tag{2}$$

with $Y_{l,m}(\theta,\phi)$ and δ_{m0} correspond to a normalized spherical harmonic function and the Kronecker symbol, respectively.

For each point of the radial grid, a least-squares procedure is performed to compute the coefficients of the development on the angular functions. In the expansion, consideration is given to the full set of m values ($0 \leqslant m \leqslant l$) for l ranging from 0 to 11, whereas we considered $m_{\max} = 6$ for $l_{\max} = 12$. This gives a total of 85 angular expansion coefficients $v_{lm}(R)$. The quality of the fit is controlled by minimizing the value of the root mean square in order to ensure reproduction of the *ab initio* points with a relative error less than 0.5% for all radial values.

Table I lists the characteristics of some selected HSN-He configurations. Given are the geometries and the energies of the minima found on the HSN-He PES for $\phi = 0°$, 90°, and 180°. The global minimum of the 3D PES is located at $R = 6.15\,a_0$, $\theta = 103°$, and $\phi = 0°$ with a well depth of $V = -74.39$ cm^{-1}. For $\phi = 0°$, two other local minima are located for $R = 7.15\,a_0$ and $\theta = 5°$ ($V = -45.04$ cm^{-1}) and for $R = 8.35\,a_0$ and $\theta = 180°$ ($V = -25.09$ cm^{-1}). For $\phi = 90°$ and 180°, the potential wells along R and θ are less deep than those described for $\phi = 0°$: at $R = 7.15\,a_0$, $\theta = 0°$, and $\phi = 180°$ the depth of the local minimum is -44.33 cm^{-1}; and at $\theta = 0°$, $\phi = 90°$, and $R = 7.15\,a_0$, the depth of this potential well is -44.33 cm^{-1}.

Figure 2 depicts the two-dimensional cuts of the 3D PES of HSN-He along the R and θ coordinates for three selected configurations ($\phi = 0°$, $\phi = 90°$, and $\phi = 180°$) and along the angular coordinates (ϕ, θ) for $R = 6.15\,a_0$ and along R and ϕ for $\theta = 103°$. These cuts show that the R stretch coordinate is strongly coupled with θ and ϕ and that the angular coordinates are also coupled together. These couplings result in strong anisotropy of the potential along the Jacobi coordinates, which should induce large rotational (de-)excitation collisional rates for HSN colliding with He. Figure 2 reveals also that the minima described above are separated by transition states. Interestingly, all these transition states are located below the dissociation energy to form HSN($\tilde{X}\,^1A$) + He products. Accordingly, the levels located above these isomerization barriers are bound and may exhibit large-amplitude motions. Finally, the comparison of the 3D PES of HSN-He to that of the isomeric form HNS-He [10] reveals that the HSN-He, like HNS-He, has in its turn a symmetric trend dependent upon the value of ϕ and possesses deeper potential wells.

III. COLLISION CROSS SECTIONS AND RATE COEFFICIENTS FOR THE HSN-He SYSTEM

A. Dynamical calculation details

At present, collisions between an asymmetric-top molecule (HNS) and a spherical atom (He) are considered. The rotational Hamiltonian of the HSN molecule is given by

$$H_{\rm rot} = \frac{j_x^2}{2I_x} + \frac{j_y^2}{2I_y} + \frac{j_z^2}{2I_z} - D_J j^4 - D_{JK} j^2 j_z^2 - D_K j_z^4 \tag{3}$$

where $I_\alpha(\alpha = x,y,z)$ are the principal moments of inertia with respect to the principal axes of inertia (Gx), (Gy), and (Gz) of HSN. (G,x,y,z) is the body-fixed reference, related to the space-fixed reference (G,X,Y,Z) by the Euler angles. I_x, I_y, and I_z are related to the rotational constants according to $A = 1/2I_x$, $B = 1/2I_y$, and $C = 1/2I_z$. The total angular momentum of the molecule is such that $j^2 = j_x^2 + j_y^2 + j_z^2$. D_J, D_{JK}, and D_K are first-order centrifugal distortion corrections. The rotational wave function $|j\tau m\rangle$ of an asymmetric-top molecule can be defined by three quantum numbers j, τ, m and can be expressed as a linear combination of the rotational wave functions $|j\tau m\rangle$ of a symmetric-top

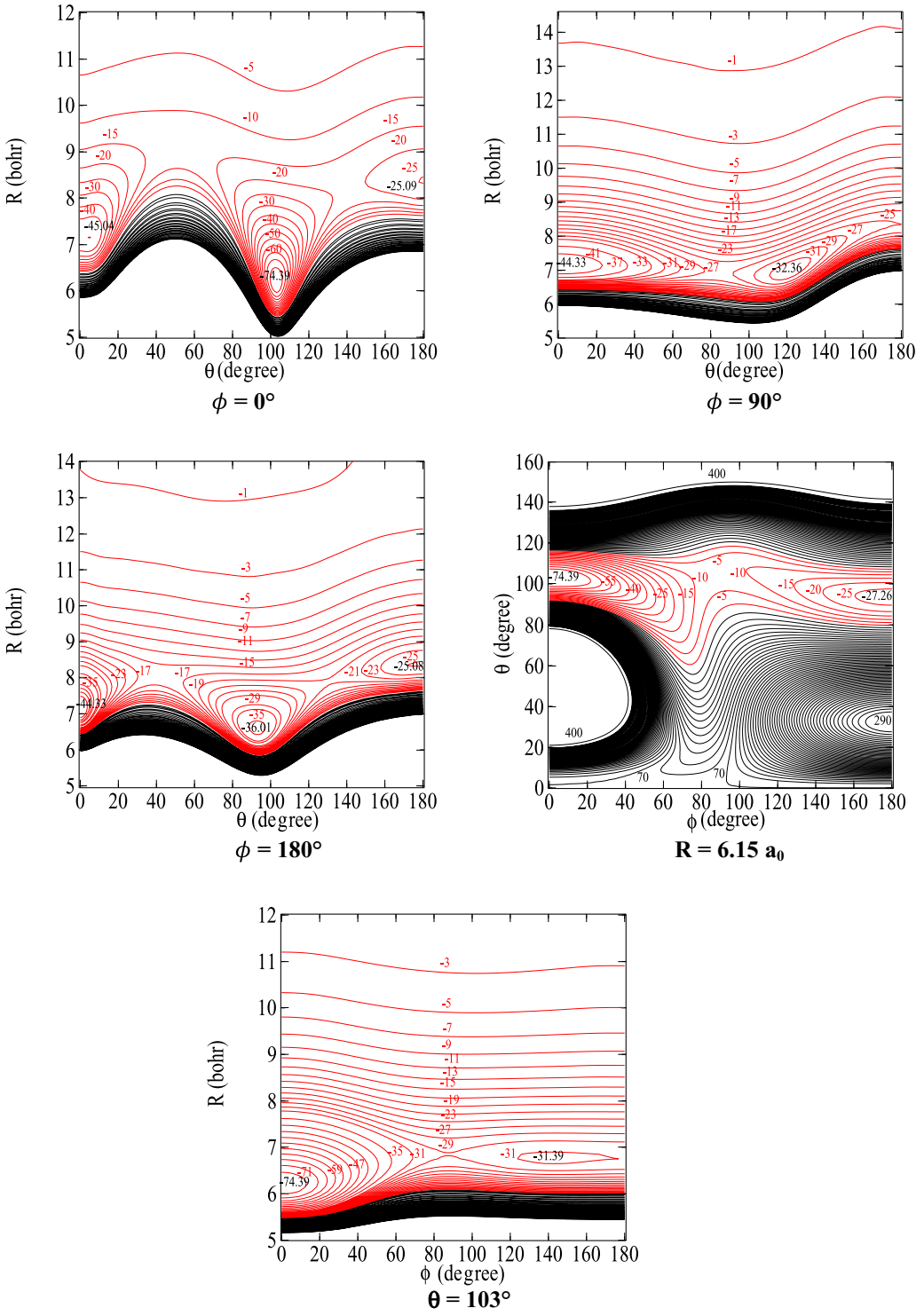

FIG. 2. Two-dimensional contour plots of the 3D HSN-He PES along the R and θ coordinates for fixed $\phi = 0°$, 90°, and 180°. We give also the cuts along the angular coordinates $R = 6.15\,a_0$ and along R and ϕ for $\theta = 103°$. Energies are in cm^{-1}. Black (red) contour lines represent repulsive (attractive) interaction energies.

molecule such as [26]:

$$|j\tau m\rangle = \sum_{k=-j}^{j} a_{\tau k}^{j} |jkm\rangle, \tag{4}$$

where j, k, and m denote the rotational quantum number, its projection along the molecular z axis, and its projection along the space-fixed Z axis, respectively; and τ is a pseudo-quantum-number that varies between $-j$ and j. The rotational levels of an asymmetric-top molecule are conventionally labeled $j_{K_a K_c}$ (adopted hereafter), where K_a and K_c are the

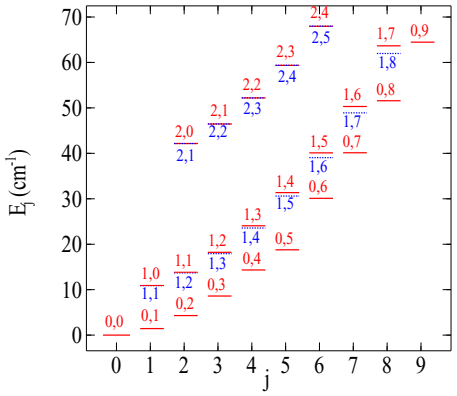

FIG. 3. HSN rotational levels for $j_{K_a K_c}$ up to 9_{09}. These levels are labeled by the values of the rotational quantum number j (given along the abscissa) and the projection quantum numbers K_a and K_c.

projections of the rotational angular momentum along the axis of symmetry in the cases of the prolate and oblate symmetric-top limits, and are related to τ through $\tau = K_a - K_c$.

The rotational energy levels $E_{j_{K_a K_c}} \equiv E_{j\tau}$ of HSN are computed from the *ab initio* rotational and distortional constants calculated by Ben Yaghlane *et al.* [9] at the CCSD(T)-F12 and cc-pVQZ-F12 level of theory, which are $A_e = 0.692$, $B_e = 0.742$, $C_e = 10.186$, $D_J = 1.0 \times 10^{-6}$, $D_K = 3.22 \times 10^{-5}$, $D_{JK} = 1.22 \times 10^{-3}$ (all values are in cm^{-1}). No rovibrational spectra for HSN species have apparently been measured so far. For scattering calculations, only the first 36 levels of the HSN molecule are considered. This corresponds to a maximum of rotational energy $E_{\mathrm{rot}} \leqslant 70\,\mathrm{cm}^{-1}$, i.e., up to $j_{K_a K_c} = 9_{09}$ ($E_{\mathrm{rot}} = 67.97\ \mathrm{cm}^{-1}$). For illustration, the diagram corresponding to these rotational levels is presented in Fig. 3. Since this molecule is relatively heavy, this diagram reveals that the rotational structure is very complex with a high density of rotational levels and with relatively small energy spacing between these levels. Shown in Table II are the frequencies for some selected dipole-allowed transitions. The dipole moment of HSN is estimated at the CCSD(T) and aug-cc-pVTZ level of theory using the finite-field method to be $\mu_x = 0.6083$, $\mu_y = 0.00$, $\mu_z = -2.5834$ (in [debye(D)]).

The analytical expansion of the 3D PES of HSN-He is incorporated into dynamical computations using the close-coupling (CC) method [27] and the coupled-states (CS) approach [28] as implemented in the MOLSCAT program. These dynamical computations are carried out for total collisional energies ranging from 1.44 up to $1400\,\mathrm{cm}^{-1}$, thus enabling the calculation of converged rate coefficients for the range of temperatures $T = 5{-}200$ K, between the first 36 rotational levels of HSN. The CC method is used for total energies of the complex up to $100\,\mathrm{cm}^{-1}$. Beyond this value, i.e., for energies from $100\,\mathrm{cm}^{-1}$ up to $1400\,\mathrm{cm}^{-1}$, the CS approximation is employed. To account for resonances during the calculations, the energy is carefully spanned over the energy range as follows: for $E < 100\,\mathrm{cm}^{-1}$, the energy step is set to $0.1\,\mathrm{cm}^{-1}$, for $100 \leqslant E \leqslant 400\,\mathrm{cm}^{-1}$ it is set to $1\,\mathrm{cm}^{-1}$, for $400 \leqslant E \leqslant 1000\,\mathrm{cm}^{-1}$ to $5\,\mathrm{cm}^{-1}$, and for $1000 \leqslant E \leqslant 1400\,\mathrm{cm}^{-1}$ to $50\,\mathrm{cm}^{-1}$. The log-derivative propagator of Manolopoulos [29] is used to solve the coupled equations.

TABLE II. Frequencies (in GHz) for some selected dipole-allowed transitions of the HSN-He system. The precision on these estimates is ~ 0.1 GHz.

Transition $j_{K_a K_c}$–$j'_{K'_a K'_c}$	Frequency
1_{01}-0_{00}	43.01
1_{11}-0_{00}	326.30
1_{10}-0_{00}	327.80
2_{12}-1_{11}	84.53
2_{02}-1_{01}	86.03
2_{12}-1_{01}	367.81
3_{13}-2_{12}	126.79
3_{03}-2_{02}	129.03
3_{13}-2_{02}	408.58
4_{14}-3_{13}	169.05
4_{04}-3_{03}	172.01
4_{14}-3_{03}	448.60
5_{15}-4_{14}	211.29
5_{05}-4_{04}	214.96
5_{15}-4_{04}	487.88

Since the size of the coupled equations and the necessary computer time for their resolution increase rapidly with the size of the basis set, a series of calculations is performed for all ranges of scattering energies in order to test the convergence of the inelastic collision cross sections with respect to the rotational basis size. These tests showed that $j_{\max} = 12$ for total energies $E \leqslant 100\ \mathrm{cm}^{-1}$, $j_{\max} = 13$ for $100 \leqslant E \leqslant 400\,\mathrm{cm}^{-1}$, and $j_{\max} = 15$ for $400 \leqslant E \leqslant 1400\,\mathrm{cm}^{-1}$ are enough to establish convergence within a few percent. In addition, rotational levels are capped at $E_{\max} = 200\ \mathrm{cm}^{-1}$ for $E \leqslant 100\,\mathrm{cm}^{-1}$, at $E_{\max} = 300\ \mathrm{cm}^{-1}$ for $100 \leqslant E \leqslant 400\,\mathrm{cm}^{-1}$, and at $E_{\max} = 400\ \mathrm{cm}^{-1}$ for $400 \leqslant E \leqslant 1400\,\mathrm{cm}^{-1}$, since a given j rotational number spans a large amount of rotational energy. These $E_{\max}$ (cutoff energies) are sufficient to converge cross sections for rotational levels up to $j_{K_a K_c} = 9_{09}$. A cutoff procedure removes some highly excited states that formally become open but in practice remain very weakly populated by transitions from the lowest states. The maximum value of the total angular momentum J_{tot} is set large enough to ensure the convergence of the inelastic cross sections to within $0.01\ \mathrm{Å}^2$.

The use of both CC and CS approaches is due to the complexity of calculations dealing with asymmetric-top-atom systems. Indeed, the determination of HSN-He cross sections using the exact close-coupling method is very CPU consuming, as it relates to the complexity associated with the increase of the number of channels in the CC equations to be solved at high collisional energies. To reach the highest rotational states, the coupled-states approach approximation is used instead for the upper collision energies. Previous studies showed that the CS approach represents a good approximation for the considered ranges of total energies [30–32]. This is also confirmed as shown in Fig. 4, which presents a close comparison of the CC and CS cross sections for some transitions and for total collisional energies $1.44 \leqslant E \leqslant 100\,\mathrm{cm}^{-1}$. Indeed, this figure

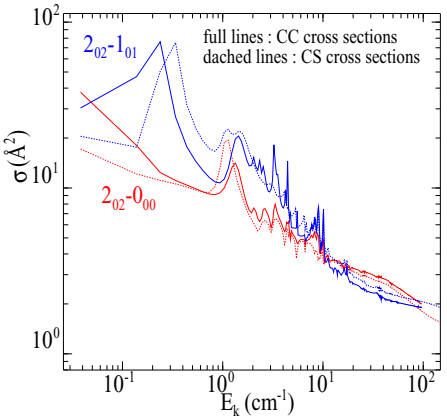

FIG. 4. Comparison between CC (dashed lines) and CS (solid lines) cross sections for selected transitions as a function of kinetic energy E_k.

shows that the cross-section shapes, magnitudes, and positions of the resonances are quite similar and well reproduced with the CS approximations, and the agreement improves with increasing collision energy (∼12% for total energy greater than 100 cm^{-1}). Therefore, we adopt the CS approximation for total collision energies $E > 100\,cm^{-1}$. Finally, in order to obtain a set of rate coefficients as accurate as possible, the CS cross sections are scaled at 100 cm^{-1} to match CC cross sections so that both values of the cross sections coincide.

B. Collision cross sections

Figure 5 illustrates the typical kinetic-energy dependence of the present calculated deexcitation cross sections associated with rotational transitions of HSN characterized by $\Delta j = (-5, -4, -3, -2, -1)$, $\Delta K_a = (-1, 0)$, and $\Delta K_c = (-5, -4, -3, -2, -1, 0, 1)$. It appears that these deexcitation cross sections share a similar shape. Indeed, they decrease quickly with increasing kinetic energy. For collision energies up to 100 cm^{-1} (i.e.,approximately the depth of the HSN-He potential), many resonances are found. These are a consequence of the quasibound states arising from tunneling through the centrifugal energy barrier (shape resonances), or from the presence of an attractive potential well that allows the He atom to be temporarily trapped in the well and hence quasibound states to be formed (Feshbach resonances) before the complex dissociates [33]. It is interesting to note that the resonances decrease in number and height with increasing j and Δj and do not exist for cross sections involving levels with large Δj due to the large threshold energy value. The first row of Fig. 5 shows that the deexcitation cross sections decrease with increasing Δj. Note that such behavior of cross sections has been observed for the HNS-He collision system. Here, it is worth noting that the HNS-He system exhibits a favored set of transitions corresponding to $|\Delta j = 2|$, $\Delta K_a = 0$, and $\Delta K_c = \Delta j$ (the transition 5_{05}-3_{03} dominates the 5_{05}-4_{04} one), like its isomeric form HSN-He. As we pointed out in Ref. [10], these propensity rules for even or odd Δj are found in the case of diatomic and linear molecules colliding with He or H_2 and have been explained in Refs. [34–38]. When the anisotropy of the potential-energy surface with respect to the He approach is weak, the transitions with even Δj are favored, whereas the transitions with odd Δj are favored when the potential is strongly anisotropic. Please note also that the strongest cross sections are those that connect levels with $\Delta K_c = 0$ as already found for an asymmetric-top molecule in collision with atoms [39].

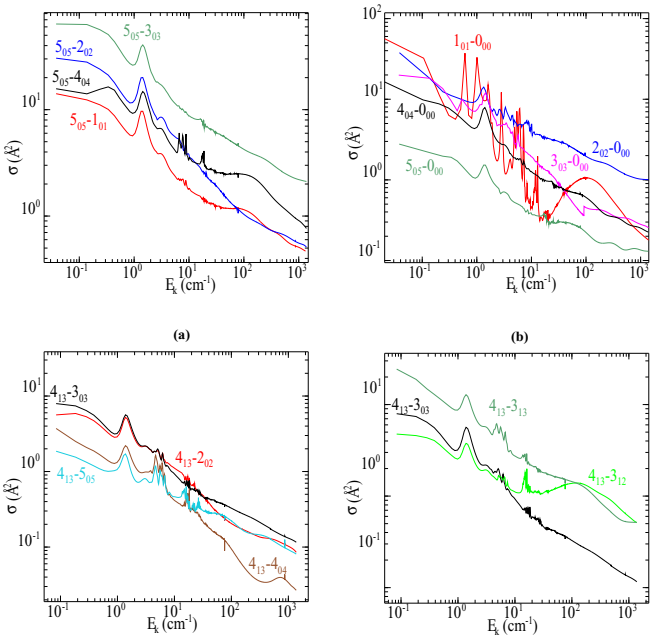

FIG. 5. Typical rotational deexcitation cross sections for collision of HSN He as a function of kinetic energy E_k. We present those for $\Delta j = (-5, -4, -3, -2, -1)$, $\Delta K_a = (-1, 0)$, and $\Delta K_c = (-5, -4, -3, -2, -1, 0, 1)$. These cross sections are computed using the CC approach for $E < 100\,cm^{-1}$ and the CS approximation for $E > 100\,cm^{-1}$.The CS cross sections are scaled and matched to the CC calculations at collision energy $E = 100\ cm^{-1}$.

C. Rate coefficients

The collisional deexcitation rate coefficients between initial and final rotational levels $j_{K_a K_c}$ and $j'_{K'_a K'_c}$ are calculated by averaging the cross sections over the Maxwell-Boltzmann distribution that describes the distribution of kinetic energies of the molecules in the gas at a given kinetic temperature (see [10]). The cross sections for total collisional energies ranging from 1.26 to 1400 cm^{-1} lead to converged rate coefficients for the first 36 rotational levels of the HSN molecule for temperatures ranging from 5 to 200 K. The complete set of (de-)excitation rate coefficients between the rotational levels will be deposited in the LAMDA [40] and BASECOL [41] databases, and can be sent upon request to the authors. For illustration, Fig. 6 depicts the rotational deexcitation rate coefficients of HSN after collision with He as a function of kinetic temperature for $j_{K_a=0,K_c=j} - 0_{00}$ (with $1 \leqslant j \leqslant 5$) transitions. Obviously, the rate coefficients display the same propensity rules as do the cross sections, and the strongest ones are those with to $|\Delta j = 2|$, $\Delta K_a = 0$, and $\Delta K_c = \Delta j$.

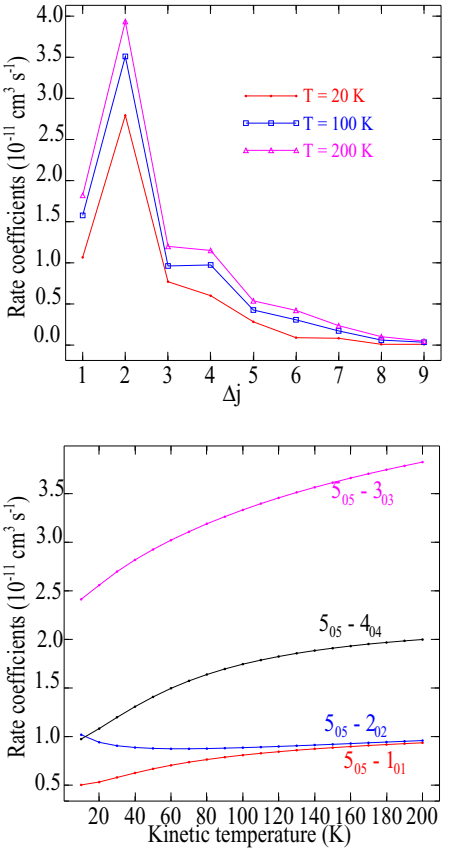

FIG. 6. Rotational deexcitation rate coefficients of HSN after collision with He as a function of kinetic temperature for $j_{K_a=0,K_c=j}$ -0_{00} (with $1 \leqslant j \leqslant 5$) transitions.

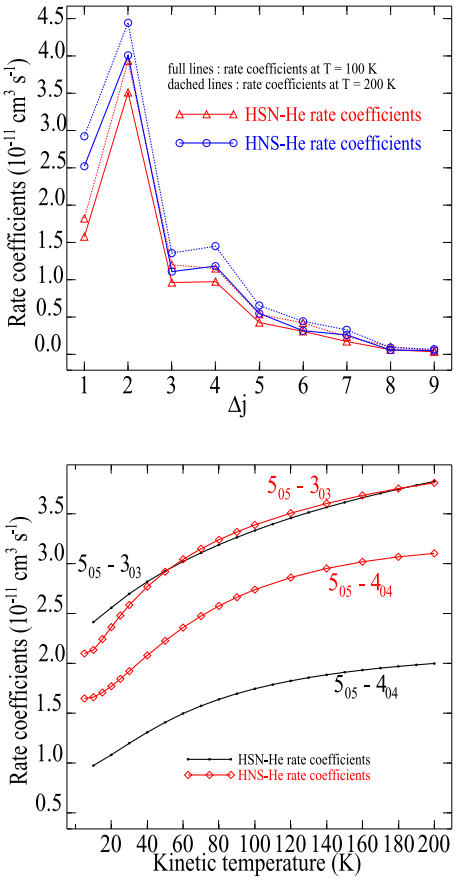

FIG. 7. HSN-He and HNS-He deexcitation rate coefficients from the 5_{05} level at 10 and 100 K.

D. Comparison of HSN-He and HNS-He results and detectability of HSN and HNS

It is interesting to compare the HSN-He rate coefficients with those of the HNS-He isomeric systems. Such a comparison should help us to determine which isomer will lead to the strongest emission lines in the interstellar spectra and thus could be more easily identified. Indeed, the magnitude of the emission lines is proportional to the population of the excited states of the molecules in the interstellar clouds. Two processes contribute to the population of the excited states: radiative and collisional processes. The magnitude of the emission lines will hence depend on both the dipole moment and the collisional rate coefficients.

Figure 7 displays the HSN–He and HNS–He deexcitation rate coefficients from the 5_{05} level at 100 and 200 K. On the whole, the HSN and HNS rate coefficients are of the same order of magnitude and display propensity rules in favor of $|\Delta j = 2|$ transitions. Note that the rate coefficients for HNS-He are slightly larger than those for HSN-He. This difference is surprising, taking into account the slightly greater well depth in the HSN-He than in the HNS-He potential-energy surface. Such behavior can, however, be explained by a stronger anisotropy in the HNS-He system which favors inelastic over elastic transitions.

More generally, such propensity rules will not help in observing these molecules in the interstellar medium (ISM) since collisions will not favor radiative transitions with $|\Delta j = 1|$ [7,37]. Indeed, the propensity rules in favor of $|\Delta j = 2|$ transitions will not favor emission lines with strong intensity. Nevertheless, the rate coefficients with $|\Delta j = 1|$ are stronger for HNS-He than for HSN-He. This information suggests that HNS will present stronger emission spectra than HSN, assuming the two molecules are present in the same environment and under similar physical environmental conditions. However, the intensity of the emission lines also depends on the dipole moment. The dipole moment of HSN ($|\mu| = 2.65$ D) is larger than that of HNS ($|\mu| = 1.48$ D [10]), leading to stronger line intensity for HSN than for HNS in the case of a similar population of the rotational states. As a consequence, it seems that HNS molecules will be more easily detected in low- to intermediate-density astrophysical media where local thermodynamic equilibrium (LTE) conditions are not reached (in the case of a competition between collisional and radiative processes for determining the population of excited states). On the other hand, in high-density astrophysical media where LTE conditions are reached, HSN lines should be more intense.

IV. CONCLUSION

The three-dimensional potential-energy surface of the HSN-He colliding system in Jacobi coordinates is generated and presented. The potential-energy surface is strongly anharmonic. Incorporation of the 3D potential-energy surface into dynamical computations to treat the nuclear motions

enabled the collision cross sections and the rate coefficients for the rotational (de-)excitation of HSN by He to be deduced. Comparisons of the collision coefficients for the rotational (de-)excitation of HNS by He suggest that HNS should be more easily detectable in interstellar cold molecular clouds (where the density is low), whereas, the emission spectra of HSN should be more intense for high-density media, and may be more easily seen in the spectral survey.

ACKNOWLEDGMENTS

The authors would like to extend their sincere appreciation to the Deanship of Scientific Research at King Saud University for funding the research through the Research Group Project No. RGP-VPP-333. This work was supported by the CNRS program "Physique et Chimie du Milieu Interstellaire" (PCMI).

[1] L. M. Ziurys, Proc Natl. Acad. Sci. U.S.A. **103**, 12274 (2006).
[2] M. A. Frerking, R. A. Linke, and P. Thaddeus, Astrophys. J. **234**, L143 (1979).
[3] D. T. Halfen *et al.*, Astrophys. J. Lett. **702**, L124 (2009).
[4] T. Trabelsi, R. Linguerri, S. Ben Yaghlane, N.-E. Jaidane, M. Mogren Al-Mogren, J. S. Francisco, and M. Hochlaf, J. Chem. Phys. **143**, 134301 (2015).
[5] T. Trabelsi, Y. Ajili, S. Ben Yaghlane, N.-E. Jaidane, M. Mogren Al-Mogren, J. S. Francisco, and M. Hochlaf, J. Chem. Phys. **143**, 034303 (2015).
[6] R. L. Pulliam, C. Savage, M. Agundez, J. Cernicharo, M. Guelen, and L. M. Ziurys, Astrophys. J. **725**, L181 (2010).
[7] M. H. Vera, F. Lique, F. Dumouchel, J. Klos, and J. R. Soneira, Mon. Not. R. Astron. Soc. **432**, 468 (2013).
[8] E. Roueff and F. Lique, Chem. Rev. **113**, 8906 (2013).
[9] S. Ben Yaghlane, N.-E. Jaîdane, C. E. Cotton, J. S. Francisco, M. M. Al Mogren, R. Linguerri, and M. Hochlaf, J. Chem. Phys. **140**, 244309 (2014).
[10] Y. Ajili, D. Ben Abdallah, M. Mogren Al-Mogren, J. S. Francisco, and M. Hochlaf, Mon. Not. R. Astron. Soc. **458**, 1581 (2016).
[11] T. B. Adler, G. Knizia, and H.-J. Werner, J. Chem. Phys. **127**, 221106 (2007).
[12] G. Knizia, T. B. Adler, and H. Werner, J. Chem. Phys. **130**, 054104 (2009).
[13] T. H. Dunning, J. Chem. Phys. **90**, 1007 (1989).
[14] R. A. Kendall, T. H. Dunning, and R. J. Harrison, J. Chem. Phys. **96**, 6796 (1992).
[15] A. Faure, P. Valiron M. Wernli, L. Wiesenfeld, C. Rist, J. Noga, and J. Tennyson, J. Chem. Phys. **122**, 221102 (2005).
[16] H.-J. Werner, P. J. Knowles, G. Knizia, F. R. Manby, M. Schütz, P. Celani, T. Korona, R. Lindh, A. Mitrushenkov, G. Rauhut, K. R. Shamasundar, T. B. Adler, R. D. Amos, A. Bernhardsson, A. Berning, D. L. Cooper, M. J. O. Deegan, A. J. Dobbyn, F. Eckert, E. Goll, C. Hampel, A. Hesselmann, G. Hetzer, T. Hrenar, G. Jansen, C. Köppl, Y. Liu, A. W. Lloyd, R. A. Mata, A. J. May, S. J. McNicholas, W. Meyer, M. E. Mura, A. Nicklaß, D. P. ONeill, P. Palmieri, K. Pflüger, R. Pitzer, M. Reiher, T. Shiozaki, H. Stoll, A. J. Stone, R. Tarroni, T. Thorsteinsson, M. Wang, and A. Wolf, MOLPROversion 2012, a package of *ab initio* programs, http://www.molpro.net.
[17] K. E. Yousaf and K. A. Peterson, J. Chem. Phys. **129**, 184108 (2008).
[18] F. Lique, J. Klos, and M. Hochlaf, Phys. Chem. Chem. Phys. **12**, 15672 (2010).
[19] P. Halvick, T. Stoecklin, F. Lique, and M. Hochlaf, J. Chem. Phys. **135**, 044312 (2011).
[20] K. Mathivon, R. Linguerri, and M. Hochlaf, J. Chem. Phys. **139**, 164306 (2013).
[21] Y. Ajili, K. Hammami, N.-E. Jaidane, M. Lanza, Y. N. Kalugina, F. Lique, and M. Hochlaf, Phys. Chem. Chem. Phys. **15**, 10062 (2013).
[22] M. Mogren Al Mogren, O. Denis-Alpizar, D. Ben Abdallah, T. Stoecklin, P. Halvick, M.-L. Senent, and M. Hochlaf, J. Chem. Phys. **141**, 044308 (2014).
[23] Y. N. Kalugina, I. A. Buryak, Y. Ajili, A. A. Vigasin, N.-E. Jaidane, and M. Hochlaf, J. Chem. Phys. **140**, 234310 (2014).
[24] O. Denis-Alpizar, Y. Kalugina, T. Stoecklin, M. H. Vera, and F. Lique, J. Chem. Phys. **139**, 224301 (2013).
[25] S. F. Boys and F. Bernardi, Mol. Phys. **19**, 553 (1970).
[26] C. H. Townes and A. L. Schawlow, *Microwave Spectroscopy* (McGraw-Hill, New York, 1955).
[27] A. M. Arthurs and A. Dalgarno, Proc. R. Soc. A **256**, 540 (1960).
[28] P. McGuire and D. J. Kouri, J. Chem. Phys. **60**, 2488 (1974).
[29] D. E. Manolopoulos, J. Chem. Phys. **85**, 6425 (1986).
[30] K. Hammami, F. Lique, N.-E. Jaidane, Z. Ben Lakhdar, A. Spielfiedel, and N. Feautrier, Astron. Astrophys. **462**, 789 (2007).
[31] L. Wiesenfeld and A. Faure, Mon. Not. R. Astron. Soc. **432**, 2573 (2013).
[32] F. Daniel, A. Faure, L. Wiesenfeld, E. Roueff, D. C. Lis, and P. Hily-Blant, Mon. Not. R. Astron. Soc. **444**, 2544 (2014).
[33] L. N. Smith, D. J. Malik, and D. Secrest, J. Chem. Phys. **71**, 4502 (1979).
[34] P. Brumer, Chem. Phys. Lett. **28**, 345 (1974).
[35] C. W. McCurdy and W. H. Miller, J. Chem. Phys. **67**, 463 (1977).
[36] D. Carty. A. Goddard, I. R. Sims, and I. W. M. Smith, J. Chem. Phys. **121**, 4671 (2004).
[37] E. Sarrasin, D. B. Abdallah, M. Wernli, A. Faure, J. Cernicharo, and F. Lique, Mon. Not. R. Astron. Soc. **404**, 518 (2010).
[38] D. Ben Abdallah, F. Najar, N. Jaidane, F. Dumouchel, and F. Lique, Mon. Not. R. Astron. Soc. **419**, 2441 (2012).
[39] B. Yang and P. C. Stancil, J. Chem. Phys. **126**, 154306 (2007).
[40] F. L. Schöier, F. F. S. van der Tak, E. F. van Dishoeck, and J. H. Black, Astron. Astrophys. **432**, 369 (2005), http://www.strw.leidenuniv.nl/~moldata.
[41] M.-L. Dubernet *et al.*, Astron. Astrophys. **553**, A50 (2013), http://basecol.obspm.fr/.